ac magnetic response of mesoscopic type-II superconductors

Alexander D. Hernández[1,2] and Daniel Domínguez[2]
[1]*Laboratorio de Superconductividad, Facultad de Física-IMRE, Universidad de la Habana, 10400, Ciudad Habana, Cuba*
[2]*Centro Atómico Bariloche and Instituto Balseiro, 8400 San Carlos de Bariloche, Río Negro, Argentina*
(Received 9 May 2002; revised manuscript received 2 August 2002; published 21 October 2002)

The response of mesoscopic superconductors to an ac magnetic field is numerically investigated on the basis of the time-dependent Ginzburg-Landau equations. We study the dependence with frequency ω and dc magnetic field H_{dc} of the linear ac susceptibility $\chi(H_{dc},\omega)$ in square samples with dimensions of the order of the London penetration depth. At $H_{dc}=0$ the behavior of χ as a function of ω agrees very well with the two-fluid model, and the imaginary part of the ac susceptibility, $\chi''(\omega)$, shows a dissipative maximum at the frequency $\nu_o=c^2/(4\pi\sigma\lambda^2)$. In the presence of a magnetic field a second dissipation maximum appears at a frequency $\omega_p \ll \nu_0$. The most interesting behavior of mesoscopic superconductors can be observed in the $\chi(H_{dc})$ curves obtained at a fixed frequency. At a fixed number of vortices, $\chi''(H_{dc})$ continuously increases with increasing H_{dc}. We observe that the dissipation reaches a maximum for magnetic fields right below the vortex penetration fields. Then, after each vortex penetration event, there is a sudden suppression of the ac losses, showing discontinuities in $\chi''(H_{dc})$ at several values of H_{dc}. We show that these discontinuities are typical of the mesoscopic scale and disappear in macroscopic samples, which have a continuous behavior of $\chi(H_{dc})$. We argue that these discontinuities in $\chi(H_{dc})$ are due to the effect of *nascent vortices* which cause a large variation of the amplitude of the order parameter near the surface before the entrance of vortices.

DOI: 10.1103/PhysRevB.66.144505 PACS number(s): 74.25.Nf, 74.20.De, 74.60.Ec, 74.25.Ha

I. INTRODUCTION

The response of superconductors to an ac magnetic field has been of interest for a long time,[1–3] and particularly in the last years.[4–14] The microwave surface impedance $Z_s=R_s-iX_s$ and the ac magnetic susceptibility $\tilde{\chi}=\chi'+i\chi''$ have been extensively studied.[1–14] Interesting behavior has been found for different values of the frequency, the magnetic field, the pinning force, and the thermal fluctuations,[4–7] whereas linear and nonlinear response appear depending on the strength of the ac signal.[7] The main interest so far has been on the electrodynamics of macroscopic samples containing a large number of vortices. In this case, it is possible to use phenomenological models to describe the macroscopic behavior of the superconducting samples.[4–7]

Recently there has been an increasing interest in the study of vortex physics on a mesoscopic scale,[15–29] a regime in which a small number of vortices are confined in a small sample. The behavior of mesoscopic superconductors is different from the behavior of bulk samples. In mesoscopic superconductors surface effects[30] are very important since the interaction of vortices with the surface currents is large.[29] The magnetic properties strongly depend on the sample sizes and geometry.[22,23,29] The most studied geometries are the the mesoscopic disk,[15,18–26] the mesoscopic slab,[16,17] and the mesoscopic square.[27–29] In particular, the mesoscopic samples can develop Abrikosov multivortex states[21] and depending on the size of the sample it is possible to observe first- or second-order transitions.[20] The electric charge of vortices,[25] a paramagnetic effect,[18,26] and the surface barrier[29,30] on a mesoscopic scale have also been studied. One interesting characteristic of the magnetic properties of mesoscopic superconductors is the behavior of the dc magnetization curves. In a mesoscopic scale, the vortices that are inside the sample induce a reinforcement of the surface barrier at fields greater than the first penetration field H_p.[29] These barriers allow for the existence of metastable states of constant vorticity as a function of magnetic field. Each metastable state becomes unstable at the ith penetration field H_{pi} in which vortices enter the sample and the magnetization has a discontinuous jump. These jumps have been observed numerically[16,20,29] and experimentally in mesoscopic Al disks.[20]

In the last years numerical simulations of the time-dependent Ginzburg Landau (TDGL) equations have been an important tool in the study of the static and dynamic properties of superconductors.[16,31–40] The TDGL model has been used to study the flux growth dynamics,[31,32] the magnetic response,[16,33] and the I-V characteristics of superconducting samples.[34] In particular, Enomoto *et al.*[38] using the TDGL equations studied the temperature dependence of the ac susceptibility at a fixed frequency in the absence of a dc magnetic field for a large sample. For increasing temperature they found that χ' exhibits a steplike change from a negative value ($\chi'=-1/4\pi$) to zero, while χ'' initially rises from zero, goes through a maximum, and then returns to a small value near T_c, which is qualitatively consistent with the overall behavior observed in experiments.

In this paper we perform numerical simulations of the time-dependent Ginzburg-Landau equation to study the ac magnetic response of type-II superconductors on a mesoscopic scale. We study the frequency and H_{dc} dependence of the linear ac susceptibility $\tilde{\chi}(H_{dc},\omega)=\chi'(H_{dc},\omega)+i\chi''(H_{dc},\omega)$ of square samples with dimensions of the order of the London penetration depth λ_L. Our results were obtained in the absence of bulk pinning and in the linear regime.

The paper is organized as follows. In Sec. II we review the known results for the ac magnetic response of macroscopic superconductors, in order to later compare them with our results in mesoscopic samples. In particular, the two-

fluid model for the Meissner state and the Coffey and Clem model for the mixed state are reviewed. In Sec. III we describe the TDGL equations used in the simulations. In Sec. IV we present our numerical results for the ac magnetic response of mesoscopic square samples. Section IV A is devoted to the study of the frequency dependence of χ' and χ''. We find that for $H_{dc}=0$ the behavior of the sample is well described by the two-fluid model. At $\omega=\nu_o=c^2/(4\pi\sigma\lambda^2)$ a maximum in the imaginary part of $\tilde{\chi}(\omega,0)$ appears. In the Meissner state for $H_{dc}\sim H_p$, another maximum appears in $\chi''(\omega)$. This behavior, characterized by the presence of two dissipation maxima is also observed in the mixed state. At the same time, for increasing frequency $\chi'(\omega,H_{dc})$ changes from London screening to a perfect diamagnetic state at high frequency. This transition is due to a decrease of the ac penetration length. In Sec. IV B we study the H_{dc} dependence of χ' and χ'' at a fixed frequency. Depending on the sample size, we find well-defined mesoscopic and macroscopic behaviors. For mesoscopic samples we observe that, in the magnetic field ranges in which the number of vortices is constant, $\chi''(H_{dc})$ continuously increases for increasing H_{dc}. At the ith vortex penetration field H_{pi}, the entrance of vortices produces a considerable suppression of the ac losses and $\chi''(H_{dc})$ decreases with a discontinuous jump. On the contrary, samples of macroscopic sizes show a continuous behavior in $\tilde{\chi}(H_{dc})$, with $\chi''(H_{dc})$ monotonically increasing with H_{dc}. In Sec. V we study the time evolution of the order parameter in mesoscopic superconductors. We show that at high frequencies and in mesoscopic samples, the vortices are fixed and only play a secondary role in the ac response of the sample. We show that the main dissipation mechanism in mesoscopic superconductors is due to the effect of ''nascent vortices.'' They cause large variations of the amplitude of the order parameter at the boundary of the sample before the entrance of vortices. Finally in Sec.VI we give a summary of our results and conclusions.

II. AC RESPONSE OF MACROSCOPIC SAMPLES: REVIEW OF KNOWN RESULTS

A. Two-fluid model and Coffey and Clem model

When an ac magnetic field is applied $H(t)=H_{dc}+h_{ac}\cos(\omega t)$, an effective complex penetration depth $\tilde{\lambda}(\omega)$ can be defined assuming that the fluctuating field inside a semi-infinite sample for $x>0$ has the form

$$\delta H = h_{ac} e^{-x/\tilde{\lambda}(\omega)} e^{-i\omega t} \tag{1}$$

or from a generalization of London's expression for the current,

$$\nabla\times\mathbf{J}(\omega) = -\frac{c}{4\pi\tilde{\lambda}^2(\omega)}\mathbf{B}(\omega). \tag{2}$$

It can be related to the frequency-dependent conductivity as $\tilde{\lambda}(\omega)=\sqrt{ic^2/4\pi\omega\tilde{\sigma}(\omega)}$. In the case of a normal metal with conductivity σ_n, the complex penetration depth is directly related to the skin depth $\delta_n=\sqrt{c^2/2\pi\omega\sigma_n}$ as $\tilde{\lambda}_n=(1+i)\delta_n/2$. The complex permeability $\tilde{\mu}(\omega)$, or the complex susceptibility $\tilde{\chi}(\omega)=\chi'(\omega)+i\chi''(\omega)=[\tilde{\mu}(\omega)-1]/4\pi$, depend both on $\tilde{\lambda}(\omega)$ and also on the specific shape of the sample, since the ac penetration of magnetic fields is a surface phenomenon. In the case of a square sample of size $L\times L$ an approximate expression for the permeability in the limit $\tilde{\lambda}\ll L$ is

$$\tilde{\mu}_{square}\approx\frac{4\tilde{\lambda}}{L}\left(1-\frac{\tilde{\lambda}}{L}\right). \tag{3}$$

Exact expressions for $\tilde{\mu}$ for squares, cylinders, and slabs can be found, for example, in Ref. 4. Sometimes the complex surface impedance Z_s is used, it can be defined when $\tilde{\lambda}\ll L$ as $Z_s=R_s-iX_s=i\omega(4\pi/c^2)\tilde{\lambda}(\omega)$.

In the Meissner state the ac response has been usually described with the two-fluid model.[41,42] In the mixed state, the magnetic flux enters in the form of quantized vortices. Therefore the dynamics of the vortices has been included in the description of the magnetic ac response of the mixed state.[4–7] In particular, Coffey and Clem have extended the two-fluid model by including the equation of motion of vortices for small displacements.[4] Similar results were obtained by Brandt[5] and by van der Beek *et al.*[7] All these models assume that there is a large number of vortices in the sample and a continuous description of the vortex lattice is used (valid for $B\gg H_{c1}$).

The two-fluid model consists in writing the total current as the sum of the supercurrent and the normal current,

$$\mathbf{J}=\mathbf{J}_s+\mathbf{J}_n, \tag{4}$$

with

$$\mathbf{J}_n=\sigma_n\mathbf{E}=-\frac{\sigma_n}{c}\frac{\partial\mathbf{A}}{\partial t}, \tag{5}$$

and the supercurrent given by the London model,

$$\nabla\times\mathbf{J}_s=-\frac{c}{4\pi\lambda_L^2}(\mathbf{B}-\mathbf{b}_v). \tag{6}$$

Here λ_L is the static London penetration depth and $\mathbf{b}_v$ is the local vortex magnetic field. In the absence of vortices, $\mathbf{b}_v=0$, the two-fluid model has the characteristic time $t_0=4\pi\lambda_L^2\sigma_n/c^2$ for the transformation of supercurrents into normal currents, since $\mathbf{J}_n=t_0\partial\mathbf{J}_s/\partial t$. The Coffey and Clem model includes the equation of motion of vortices for small displacements $\mathbf{u}(\mathbf{x},t)$ from their equilibrium positions,

$$\eta_v\dot{\mathbf{u}}+\kappa_p\mathbf{u}=\frac{1}{c}\mathbf{J}_s\times\Phi_0\hat{\boldsymbol{\alpha}} \tag{7}$$

where η_v is the viscous drag coefficient, κ_p is the restoring force constant (Labusch parameter) of a pinning potential well, and $\hat{\boldsymbol{\alpha}}$ the local vortex direction. Here we have neglected thermal fluctuation effects. The small vortex displacements induce perturbations of the local vortex magnetic field, $\mathbf{b}_v+\delta\mathbf{b}_v$, which depend as $\delta\mathbf{b}_v=\nabla\times(\mathbf{u}\times\mathbf{B})$.[7]

In the case of fields $\mathbf{H}\|\mathbf{h}_{ac}$ and parallel to the surface, using Eqs. (2) and (4)–(7) the effective complex penetration depth[4] can be obtained as

$$\tilde{\lambda}^2=\lambda_L^2\frac{1+\left(\frac{\lambda_L^2}{\lambda_C^2}-i\omega t_{ff}\right)^{-1}}{1-i\omega t_0}=\frac{\lambda_L^2+\left(\frac{1}{\lambda_C^2}-i\frac{2}{\delta_{ff}^2}\right)^{-1}}{1-i\frac{2\lambda_L^2}{\delta_n^2}} \quad (8)$$

with the Campbell penetrationd depth $\lambda_C^2=B\Phi_0/4\pi\kappa_p$, the flux-flow time scale $t_{ff}=4\pi\lambda_L^2\sigma_{ff}/c^2$, the flux-flow conductivity $\sigma_{ff}=c^2\eta_v/B\Phi_0$, and the flux-flow skin depth $\delta_{ff}^2=c^2/2\pi\omega\sigma_{ff}$. Since $\sigma_{ff}\sim\sigma_n H_{c2}/B$, we have $\sigma_{ff}>\sigma_n$ and $t_{ff}>t_0$. Therefore the highest characteristic frequency is $\nu_0=1/t_0$, which for conventional superconductors is about $\nu_0\sim 10$–100 GHz.[43]

B. Meissner state

In the absence of vortices the complex penetration depth is simply $\tilde{\lambda}^2=\lambda_L^2/(1-i\omega t_0)$. This leads to a dissipation peak in χ'' when $\omega t_0\approx 1$. For large frequencies, $\omega t_0\gg 1$ (i.e., $\delta_n\ll\lambda_L$), the system behaves as a normal metal (normal-state skin depth effect) with

$$\lambda'=\lambda''\approx\lambda_L\sqrt{\frac{1}{2\omega t_0}}. \quad (9)$$

Therefore dissipation goes as $\chi''\propto\lambda''/L\sim\omega^{-1/2}$ for large ω. For low frequencies, $\omega t_0\ll 1$ (i.e., $\delta_n\gg\lambda_L$), the system is dominated by the Meissner effect and

$$\lambda'\approx\lambda_L,\quad \lambda''\approx\lambda_L\frac{1}{2}\omega t_0, \quad (10)$$

and therefore dissipation goes as $\chi''\propto\lambda''/L\sim\omega$ for low ω.

C. Vortices without pinning

In the presence of vortices, the interesting frequency range is $\omega t_0\ll 1$ since for frequencies $\omega t_0\gg 1$ the system always behaves as in Eq. (9), corresponding to the normal-state skin depth effect.

Let us first discuss the case when there is no bulk pinning, $\kappa_p=0$ ($\lambda_C=\infty$). For frequencies such that $\omega t_{ff}\gg 1$, the system behaves similarly to the Meissner state, with a dissipation peak at $\omega t_0\approx 1$, as described previously. For frequencies such that $\omega t_{ff}\ll 1$ the system is dominated by the ''flux-flow skin depth effect'' due to the flux-flow conductivity σ_{ff}. In this limit $\tilde{\lambda}^2\approx i\delta_{ff}^2/2=i\lambda_L^2/\omega t_{ff}$, and therefore the susceptibility for low frequencies should diverge as $\tilde{\chi}\sim\omega^{-1/2}$. This divergence is cut off by the finite system size. At low frequencies the real part of the effective penetration depth λ' saturates to the system size L. This leads to a dissipation peak at a frequency[6]

$$\omega_L\propto\frac{c^2}{L^2\sigma_{ff}}\propto\frac{B}{L^2}, \quad (11)$$

and for very low frequencies such that $\omega\ll\omega_L$, dissipation diminishes linearly as

$$\chi''\propto\frac{\sigma_{ff}L^2}{c^2}\omega. \quad (12)$$

D. Vortices with pinning

In the presence of bulk pinning, $\kappa_p\neq 0$, the relevant time scale is $t_C=t_{ff}\lambda_C^2/\lambda_L^2=\eta_v/\kappa_p$. Now instead of the finite-size peak at ω_L, there is a vortex dissipation peak when $\omega t_C\approx 1$. It is worth mentioning that this peak frequency,

$$\omega_C\propto\frac{\kappa_p}{\eta_v}, \quad (13)$$

is independent of magnetic field. For low frequencies, $\omega t_C\ll 1$, the real part of the penetration depth tends to $\lambda'\approx\tilde{\lambda}_C=\sqrt{\lambda_C^2+\lambda_L^2}$, while the imaginary part $\lambda''\approx\omega t_C\lambda_C^2/2\tilde{\lambda}_C$. Thus for low frequencies the dissipation diminishes linearly with ω as

$$\chi''\approx\frac{1}{2\pi}\frac{\lambda_C^2}{\tilde{\lambda}_C L}\omega t_C. \quad (14)$$

Therefore in the presence of vortices there is a new dissipation peak, in addition to the ''two-fluid peak,'' either at ω_L or at ω_C depending on the importance of pinning. At low frequencies the relevant length scale for penetration of the ac field is either L (in the absence of pinning) or λ_C (if pinning is important) and the dissipation is linear with frequency in both cases.

E. Surface barrier effects

At the surface of a type-II superconductor there is a potential barrier that prevents the entrance (and the exit) of vortices. This barrier has been calculated by Bean and Livingston.[30] The surface barrier inhibits the penetration of flux at H_{c1}, where penetration is thermodynamically favorable. Instead of H_{c1}, vortices start to enter at the first penetration field $H_p>H_{c1}$. Above H_p, the Bean-Livingston surface barrier can stabilize metastable states with a nonequilibrium number of vortices.[44,45] The interval of external magnetic fields where these metastable states exist in macroscopic superconductors has been obtained in Refs. 44–46. It has been found that for fields $H>H_p$ the vortex array is separated from the boundary surface by a vortex-free region because of the effect of the surface barrier. The length of this vortex-free region[44–46] is $d_{SB}=\lambda_L\cosh^{-1}(H/B)$. The ac magnetic response has been calculated by Sonin and Traito[8] in this case. They assume that the number of vortices is fixed, and they allow the size of the vortex free region d_{SB} to fluctuate with the rf field $h_{ac}e^{-i\omega t}$. A different dissipation peak is found at a frequency

$$\omega_{SB}\approx\frac{\tanh^2(d_{SB}/\lambda_L)}{t_{ff}}, \quad (15)$$

which for $B \ll H_p$ is $\omega_{SB} \approx 1/t_{ff}$. For low frequencies $\omega \ll \omega_{SB}$, the effective penetration depth goes as

$$\lambda' \approx \lambda_L \coth\left(\frac{d_{SB}}{\lambda_L}\right), \tag{16}$$

$$\lambda'' \approx \frac{\lambda_L^2}{\sinh^2\left(\frac{d_{SB}}{\lambda_L}\right)} \sqrt{\frac{2\pi\sigma_{ff}\omega}{c^2}}.$$

Therefore, according to this approach, the dissipation should go as $\chi'' \propto \lambda''/L \sim \omega^{1/2}$ if surface barrier effects are important. Experimentally, dissipation maxima attributed to surface barriers have been measured, for example, in Ref. 47. In platelet samples with a perpendicular magnetic field, geometrical effects enhance the surface barrier, giving place to a ''geometrical barrier.'' Morozov *et al.*[48] have measured the effect of geometrical barriers in the ac response of a superconductor. In this case there is a dissipation maximum as a function of magnetic field for $H \gtrsim H_p$, which is independent of frequency.

III. MODEL AND DYNAMICS

Our numerical simulations are carried out using the time-dependent Ginzburg-Landau equations complemented with the appropriate Maxwell equations. In the zero-electric potential gauge we have[33,40]

$$\frac{\partial \Psi}{\partial t} = \frac{1}{\eta}[(\nabla - i\mathbf{A})^2\Psi + (1-T)(1-|\Psi|^2)\Psi], \tag{17}$$

$$\frac{\partial \mathbf{A}}{\partial t} = (1-T)\,\mathrm{Im}[\Psi^*(\nabla - i\mathbf{A})\Psi] - \kappa^2 \nabla \times \nabla \times \mathbf{A}, \tag{18}$$

where Ψ and $\mathbf{A}$ are the order parameter and vector potential, respectively, and T is the temperature. Equations (17) and (18) are in their dimensionless form. Lengths have been scaled in units of the coherence length $\xi(0)$, times in units of $t_0 = 4\pi\sigma_n\lambda_L^2/c^2$, $\mathbf{A}$ in units of $H_{c2}(0)\xi(0)$, and temperatures in units of T_c. η is equal to the ratio of the characteristic time t_0 for the relaxation of A and the time t_{GL} for the relaxation of Ψ: $\eta = t_{GL}/t_0 = c^2/(4\pi\sigma_n\kappa^2 D)$, with $t_{GL} = \xi^2/D$, where σ_n is the quasiparticle conductivity and D is the electron diffusion constant. For superconductors with magnetic impurities we have $D_{imp} = c^2/(48\pi\kappa^2\sigma_n)$, and therefore $\eta = 12$ in this case.

The time-dependent Ginzburg-Landau equations have been proposed[49] as a time-dependent generalization of the mean-field approach of the Ginzburg-Landau theory. Gorkov and Eliasberg[50] demonstrated that the TDGL equations can be obtained from the microscopic BCS theory in the case of gapless superconductors. In general, they are also expected to be approximately correct close to T_c where the superconducting gap is small. Moreover, experimental results frequently show that the TDGL equations are often valid in a higher range of temperature and magnetic field. In the case of mesoscopic superconductors, mesoscopic fluctuations tend to remove the singularities in the density of states. Therefore one would expect that the TDGL equations are particularly well suited to study mesoscopic systems, even not very close to T_c.

We solve numerically the TDGL equations following the same procedure as in our previous work in Ref. 29, using a standard finite difference discretization scheme.[40] We discretize space in a rectangular mesh with spacings Δx and Δy in each direction. The order parameter and vector potentials are defined at the nodes of the rectangular mesh $[\vec{r} = (I,J)]$, and the link variables $U_{\mu I,\mp} \exp(-\imath\kappa h_\mu A_{\mu I,J})$ $(\mu = x,y)$ are introduced in order to maintain the gauge invariance under discretization. We assume that the sample has a square shape in the x,y direction and it is infinite in the z direction. We apply the magnetic field parallel to the z direction, therefore the problem is reduced to two dimensions neglecting all derivatives along z. The symmetry of the problem implies for all mesh points $A_{I,J} = (A_{xI,J}, A_{yI,J}, 0)$ and $\mathbf{B}_{I,J} = (0,0,B_{zI,J})$, where $B_{zI,J} = (\nabla \times \vec{A})_z = (\partial_x A_{yI,J} - \partial_y A_{xI,J})$.

The dynamical equations must be complemented with the appropriate boundary conditions for both the order parameter and the vector potential. For the order parameter we have used the boundary condition

$$(\Pi\Psi)^\perp = (\nabla - i\vec{A})^\perp \Psi = 0, \tag{19}$$

usually known as the superconductor-insulator (S-I) boundary condition because it implies that the perpendicular component of the superconducting current is equal to zero at the surface $(\vec{J}_s^{\perp} = 0)$. This boundary condition also minimizes the free energy at the sample surface.

Our numerical approach neglects the three dimensional magnetic-field distribution, and therefore demagnetization effects are not taken into account. This is equivalent to assume that the sample is infinite in the direction of the external magnetic field (the $\hat{\mathbf{z}}$ direction). Therefore, strictly speaking, our results describe square samples that are mesoscopic only in the xy plane (perpendicular to the magnetic field) and infinite along the z axis. In this approximation, the difference in the screening magnetic fields with respect to the truly two-dimensional square samples will be more important at small fields.

The ac magnetic field is introduced in the simulation through the boundary condition for the vector potential $A_{\mu I,J}$. We consider the case where the ac magnetic field $\mathbf{h}_{ac}$ is parallel to the dc component $\mathbf{H}_{dc}$, and both fields are in the z direction:

$$B_z|_S = (\nabla \times \mathbf{A})_z|_S = H_{dc} + h_{ac}\cos(\omega t);$$

this expression is evaluated at the sample surface. We study the response of a superconductor in the linear regime, i.e., $h_{ac} \ll H_{dc}$. The time dependence of the sample magnetization can be obtained from the magnetic induction averaged over the sample $\langle B(t) \rangle$ through the relation

$$4\pi M(t) = \langle B(t) \rangle - H(t).$$

The ac magnetic susceptibilities are obtained from the Fourier transform of $M(t)$:

$$\chi'(H_{dc},\omega)=\frac{1}{\pi h_{ac}}\int_0^{2\pi} M(t)\cos(\omega t)d(\omega t),$$

$$\chi''(H_{dc},\omega)=\frac{1}{\pi h_{ac}}\int_0^{2\pi} M(t)\sin(\omega t)d(\omega t). \qquad (20)$$

In what follows, we have solved the TDGL equations numerically for a type-II superconductor with $\kappa=2$, mean-field temperature $T=0.5$, and the parameter $\eta=12$. We used a spatial discretization of $\Delta x=\Delta y=0.5\xi$ and, in order to make efficient calculations, we have chosen adequately the time step with values $\Delta t\leqslant 0.015t_0$.

IV. AC SUSCEPTIBILITY IN MESOSCOPIC SUPERCONDUCTORS

In a mesoscopic sample the behavior of the ac magnetic response in the presence of a dc magnetic field can be different than in the macroscopic case. On one hand, the models typically used for macroscopic samples (see Sec. II) assume a high density of vortices (and therefore an almost uniform magnetic-field profile inside the sample[5]), applied magnetic fields such that $H_{c1}\ll H\ll H_{c2}$, and very large (semi-infinite) samples. On the other hand, in mesoscopic samples there is a small number of vortices, surface barriers cannot be neglected, and the finite size of the sample is important. Here we perform simulations of squares samples of sizes in the range from $5\lambda\times 5\lambda$ to $20\lambda\times 20\lambda$ using the TDGL equations.

We start by showing in Fig. 1 a typical high-frequency ac magnetic response of a small sample. In Fig. 1(a) we plot the driving field $H(t)=H_{dc}+h_{ac}\cos\omega t$ and the corresponding magnetization $M(t)$ of the sample. We show the response of the system after a long equilibration time (typically around 100 periods of the external ac field). It can be observed that the magnetization has a sinusoidal behavior, which is a signal that we are in the linear regime and also that the sample is following the external perturbation. It can also be observed that there is a phase shift between the magnetization and the external field due to the presence of dissipation. Figure 1(b) shows the magnetization loop obtained from the signals of Fig. 1(a). The area inside the loop is proportional to the time average of the energy dissipated in the sample and it is proportional to the imaginary part of the ac susceptibility χ''. The appearance of dissipation changes the relationship between $M_{ac}(t)$ and $H_{ac}(t)$ and therefore the real part of the ac susceptibility, $\chi'(H_{dc},\omega)$, will depend on the frequency of the ac signal as well as on the bias field H_{dc}.

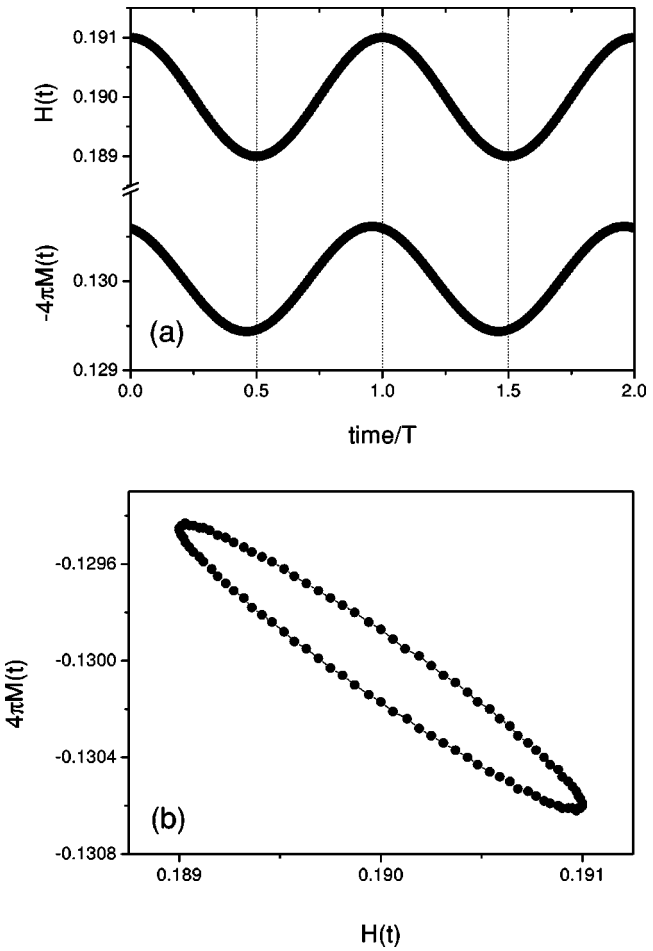

FIG. 1. Response of a superconductor to a high-frequency magnetic field. (a) Time variation of the driving field and the sample magnetization, and (b) the magnetization loop that shows the presence of dissipation inside the sample. (Sample size: $20\lambda\times 20\lambda$, $H_{dc}=0.38H_{c2}(T)$, $\omega t_0=0.028$.)

A. Frequency dependence

In order to understand the different dynamical regimes of the ac response, we study first the dependence of $\tilde{\chi}=\chi'+i\chi''$ with frequency ω for different values of the dc magnetic field H_{dc}. In Figs. 2 and 3 we show the imaginary and the real part of the susceptibility, respectively. These curves were obtained for a sample of $20\lambda\times 20\lambda$.

Figure 2(a) shows the low-frequency behavior of χ'' for several values of the magnetic field. Figure 2(b) shows the full $\chi''(\omega)$ curves obtained for fields such that there are no vortices within the sample, i.e., in the Meissner state. For fields above the first penetration field H_p, vortices enter into the sample. The full frequency dependence of $\chi''(\omega)$ in the presence of vortices, i.e., for fields $H_{dc}>H_p$, is shown in Fig. 2(c).

The simplest case to understand is the behavior when there is no external field applied, $H_{dc}=0$. In this case the complex susceptibility agrees very well, both qualitatively and quantitatively, with the two-fluid model described in Sec. II B. For low frequencies, χ'' has a linear dependence with ω as given by Eq. (10). There is a maximum in $\chi''(\omega,0)$ at $\omega=\nu_o=1/t_0$. At high frequencies $\omega\gg\nu_0$ the dissipation is due to the normal electrons and follows the expected dependence $\chi''\sim\omega^{-1/2}$ as given by Eq. (9), corresponding to the normal-state skin depth effect.

For small magnetic fields within the Meissner state, $0<H_{dc}\ll H_p$, the behavior is qualitatively similar to the $H_{dc}=0$ case, with a peak at $\omega=\nu_0$. The main difference is that the slope of the low ω linear dependence increases with magnetic field, as can be seen in Fig. 2(a). According to Eq. (10), the linear slope for low frequencies is proportional to

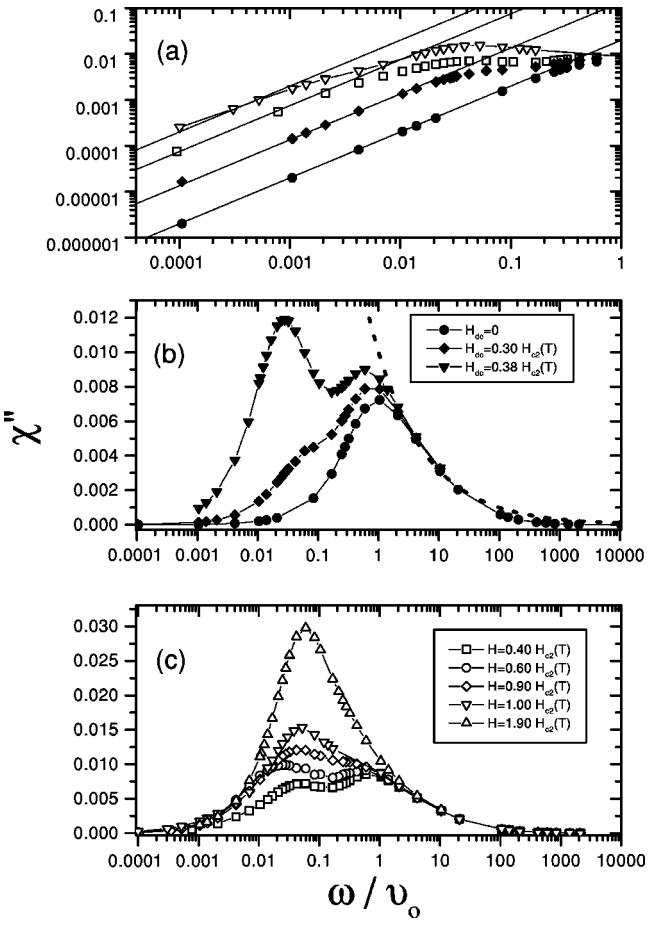

FIG. 2. Frequency dependence of the imaginary component of the ac susceptibility χ'' at different fields H_{dc}, for samples of size $20\lambda \times 20\lambda$. (a) Low-frequency behavior for fields in the Meissner state [black symbols, $H_{dc}/H_{c2}(T)=0,0.30$] and in the mixed state [open symbols, $H_{dc}/H_{c2}(T)=0.40,1.0$]. The continuous lines correspond to a linear dependence $\chi'' \sim \omega$. (b) Frequency dependence in the Meissner state (number of vortices: $N_v=0$). The dashed line corresponds to a dependence $\chi'' \sim \omega^{-1/2}$. (c) Frequency dependence in the mixed state ($N_v \neq 0$). The frequency is normalized by $\nu_o = 1/t_0$.

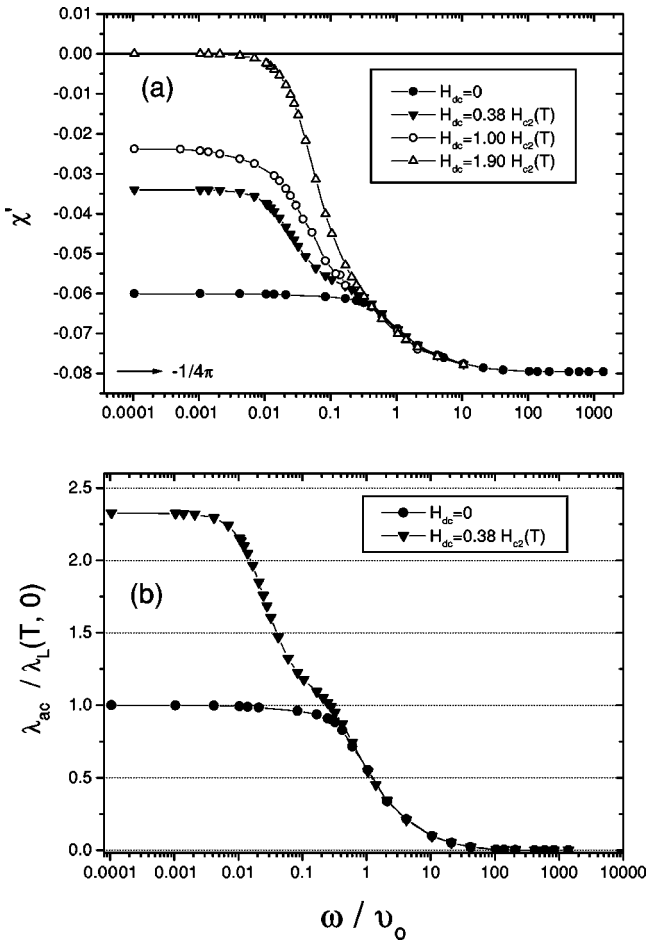

FIG. 3. (a) Frequency dependence of the real component of the ac susceptibility χ' at different values of H_{dc} (black symbols: Meissner state; open symbols: mixed state) and (b) effective ac penetration depth λ_{ac} as a function of frequency.

λ_L. This implies that the London penetration depth should be dependent on magnetic field: $\lambda_L(H)$. Also, Fig. 2(b) shows that the magnitude of $\chi''(\omega)$ at any given ω increases for increasing H_{dc}. These two effects are easily understood since the Meissner screening currents deplete the magnitude of the order parameter at the surface, which leads to a larger static penetration depth $\lambda_L(H)$ (see also Sec. IV B) and to an increase in the normal electron dissipation. The most interesting result is that for H_{dc} near but still *below* H_p a second dissipative maximum appears in $\chi''(\omega)$. This second peak is at a frequency ω_p two orders of magnitude below ν_o.

For $H_{dc} > H_p$ the vortices enter into the sample. In this case we still find a low-frequency linear dependence $\chi'' \sim \omega$, as shown in Fig. 2(a). Only for large fields close to H_{c2} a small departure from linear dependence is observed, $\chi'' \sim \omega^{\alpha}$, with $\alpha \approx 0.8$. The behavior for very large frequencies $\omega \gg \nu_0$ is the same for all magnetic fields, since it corresponds to the normal-state skin depth effect with χ'' $\sim \omega^{-1/2}$, as mentioned before. As can be observed in Fig. 2(c), the main characteristic of the mixed state is that there are two dissipation maxima as a function of frequency in $\chi''(\omega)$. The high-frequency maximum corresponds to the "two-fluid peak" at $\omega \approx \nu_0$. The low-frequency maximum that appears at a frequency $\omega_p \ll \nu_0$ is a continuation of the maximum observed when $H_{dc} \lesssim H_p$. The peak frequency ω_p shows a weak dependence with magnetic field, ω_p first decreases and then increases with increasing H_{dc}. For fields $H_{dc} \geqslant H_{c3}$ the sample is completely in the normal state and there is a single maximum in the χ'' vs ω curve. It corresponds to the frequency at which the normal-state skin depth δ_n equals the system size L.

Let us now analyze the frequency dependence of the real part of the susceptibility, $\chi'(\omega)$, which is shown in Fig. 3(a) for some values of H_{dc}. From $\chi'(\omega)$ it is possible to extract the real part of the effective ac penetration depth $\lambda_{ac} = \lambda'(\omega)$ using Eq. (3). The length λ_{ac} represents the length scale for the penetration of the ac component of the magnetic field and its frequency dependence is shown in Fig. 3(b). In the absence of a bias field ($H_{dc}=0$), $\chi'(\omega)$ is well described by the two-fluid model, as given in Eqs. (9) and (10). The sample changes from a London screening for $\omega \ll \nu_o$,

with $\lambda_{ac} \approx \lambda_L$, to a perfect diamagnetic state for $\omega \gg \nu_o$, with $\lambda_{ac} \approx 0$. At low frequencies χ' is larger than $-1/4\pi$ due to the penetration of the field in a region of size λ_L near the sample surface, $\chi' \approx (-1/4\pi)(1-4\lambda_L/L)$. At high frequency the ac penetration depth is $\lambda_{ac} \ll \lambda_L$ and $\chi'(\omega) \approx -1/4\pi$. The opposite case is for $H_{dc} = 1.9 H_{c2}(T) > H_{c3}$ with the sample mostly in the normal state (at this field the surface superconductivity disappears and there is superconductivity only at the corner of the sample[38]). As can be expected, in this case the system behaves as a normal metal and is dominated by the skin depth effect with $\lambda_{ac} \approx \delta_n/2$. For low frequencies, the skin depth δ_n equals the system size and thus $\chi' \approx 0$. For magnetic fields within the Meissner state, $0 < H_{dc} \ll H_p$, we find that for low frequencies, $\omega \ll \nu_0$, the ac penetration depth saturates to the field-dependent London penetration depth $\lambda_L(H)$, which increases with H. The most interesting case is for $H_{dc} \lesssim H_p$, which is shown in Fig. 3. In this situation, one can distinguish three frequency regimes, as it was found before in the dissipative part, $\chi''(\omega)$. At the frequencies for which there are maxima in the dissipation, ν_0 and ω_p, there is a rapid change in the value of $\chi'(\omega)$ [or in $\lambda_{ac}(\omega)$]. For $\omega \gg \nu_0$ the normal-fluid behavior of Eq. (9) is followed, as expected for all values of H_{dc}. For the frequency range $\omega_p < \omega < \nu_0$, there is a shoulder in $\chi'(\omega)$ [and $\lambda_{ac}(\omega)$], which basically corresponds to an ac penetration depth of the order of the expected value for $\lambda_L(H)$ at that field. At low frequencies, $\omega < \omega_p$, the ac penetration depth saturates to a length l_p which is smaller than the system size and larger than $\lambda_L(H)$.

In summary, the most interesting feature observed in $\tilde{\chi}(\omega)$ is the appearance of a dissipation maximum at frequencies $\omega_p(H) \ll \nu_0$ in the presence of a magnetic field. A dissipation maximum in macroscopic samples is expected when $H \neq 0$, as we discussed in Sec. II. It can be caused by several reasons: (i) finite size, (ii) surface barriers, or (iii) bulk pinning. However, the behavior predicted in any of these cases is not followed in the mesoscopic samples studied. Let us discuss each of the possibilities. (i) Finite size: in a small sample this is the first effect to analyze. The characteristic frequency for finite-size effects, ω_L, should increase linearly with B and decrease with system size, as given by Eq. (11). However, ω_p has a weak and nonmonotonous dependence with magnetic field, as seen in Fig. 2(c). In Fig. 4 we show $\chi''(\omega)$ in a smaller sample with $L = 5\lambda$ (and $\eta = 12$) for $H_{dc} \lesssim H_p$. We see that the maximum appears at the same frequency ω_p as in the $L = 20\lambda$ case for the same magnetic field [Fig. 2(b)]. Therefore ω_p has no size dependence. Furthermore, in Fig. 3 we see that when $\omega \to 0$ the sample is still diamagnetic and $\lambda_{ac} < L$ [a finite-size effect would have $\chi'(\omega \to 0) \approx 0$ and $\lambda_{ac} \gtrsim L$]. (ii) Surface barrier: in mesoscopic samples, surface barriers are very important.[29] In macroscopic samples, the effect of surface barriers, assuming a large number of vortices, gives a low-frequency dependence for dissipation as $\chi'' \sim \omega^{\alpha}$ with $\alpha = 1/2$; see Eq. (16) and Ref. 8. However, we find a linear frequency dependence in most cases as shown in the inset of Fig. 2(a), and even when there is a departure from linearity, it is with an exponent of $\alpha \approx 0.8 > 0.5$. Also the characteristic frequency ω_{SB} of Eq. (15) has a strong dependence on magnetic field, which is not observed here. (iii) Pinning: since there is no disorder in the model, no bulk pinning is expected. However, in a very small sample one may argue that, given the smallness of the system, the sample itself acts as a confinement potential for vortices. In this case, κ_p in Eq. (7) would represent the vortex elastic response for small oscillations within this confinement potential. The characteristic frequency for pinning effects, ω_C, is independent of magnetic field in macroscopic samples, according to Eq. (13). The weak-field dependence of ω_p may still be consistent with this result (the effective κ_p may depend on the number and distribution of vortices inside the sample in this hypothetic case of "confinement potential"). Also the fact that $\lambda_{ac} < L$ for $\omega \ll \omega_p$ in Fig. 3(b) is consistent with a finite "Campbell's penetration depth" λ_C (and then $l_p \equiv \lambda_C$). However, we also have to discard this possibility, since we find that there is a dissipation maximum at ω_p *even when there are no vortices in the sample*. As shown in Fig. 2(b) the dissipation peak already appears for magnetic fields just below the penetration field H_p. To be more precise, we have explicitly calculated the topological number of total vorticity as $N_v = (1/\Phi_o) \oint (A + J_s/|\Psi|^2) dl$. We obtain $N_v = 0$ at all times for the magnetic fields shown in Fig. 2(b). Therefore all arguments based on the oscillation of vortices, as for example the Coffey and Clem model[4] of Eq. (8), which work very well for macroscopic samples, are not enough to explain the dissipation maxima observed in these mesoscopic samples.

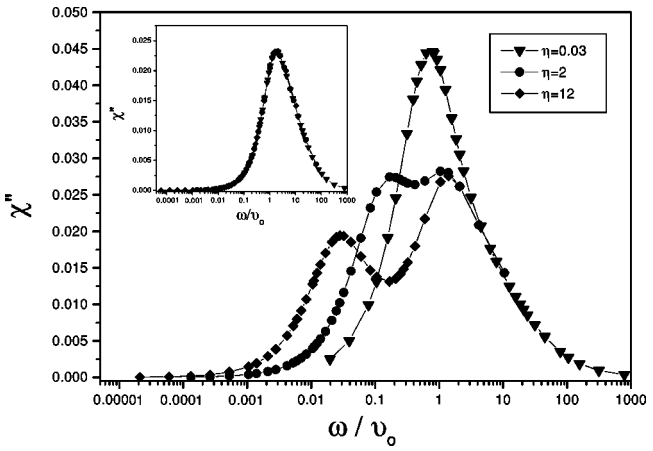

FIG. 4. Dependence with the TDGL time scale $t_{GL} = \eta t_0$. χ'' vs ω curves for small mesoscopic samples $5\lambda \times 5\lambda$ in the Meissner state ($N_v = 0$) near the penetration field, $H \lesssim H_p$, $H_{dc} = 0.35 H_{c2}(T)$. The inset shows the dependence with η for $H_{dc} = 0$.

In Fig. 4 we show that ω_p depends directly on the time scale for the relaxation of the amplitude of the order parameter, $t_{GL} = \eta t_0$. We consider a magnetic field $H_{dc} \lesssim H_p$ and we change the value of η in Eqs. (17) and (18). The "two-fluid peak" is always at the same frequency $\nu_0 = 1/t_0$, since t_0 is fixed. We find that when decreasing η, the frequency ω_p shifts to higher values and increases monotonically with $1/t_{GL}$, until the rather unphysical case of $t_{GL} < t_0$ ($\eta < 1$), when only the two-fluid peak at ν_0 is observed. The dependence of ω_p with t_{GL} shows that variations in the amplitude

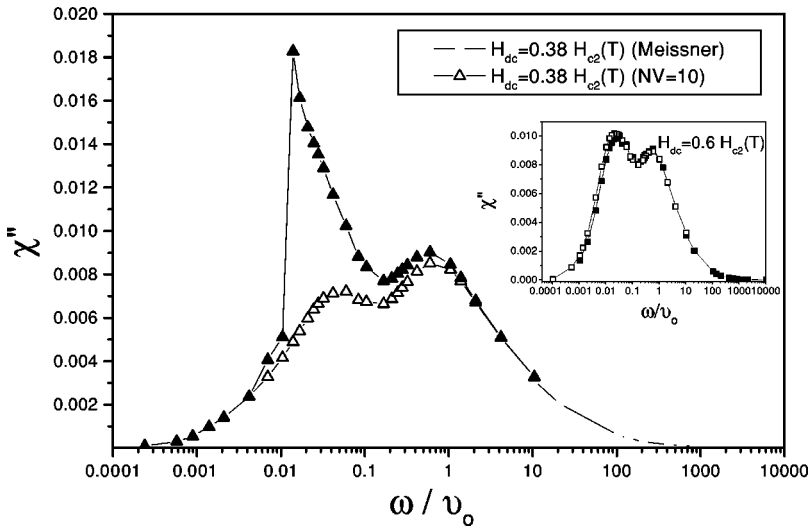

FIG. 5. History dependence of χ'' vs ω curves for H_{dc} near the penetration field H_p [$H_{dc}=0.38H_{c2}(T)$]. Black triangles: decreasing frequency from a high ω state without vortices ($N_v=0$); the branch for ω above the jump has $N_v=0$ and below the jump $N_v=10$. White triangles: increasing frequency from a low ω state with $N_v=10$. Sample size is $20\lambda\times20\lambda$. The inset shows the absence of history dependence for a larger magnetic field, $H_{dc}=0.6H_{c2}(T)$.

of the order parameter are the main mechanism of this dissipation maximum, as we will see more clearly later in Sec. V. In the inset of Fig. 4 we verify that for $H_{dc}=0$ the behavior is independent of t_{GL}, since this case can be simply described with the two-fluid model.

The appearance of the dissipation maximum for a magnetic field below H_p, just before the penetration of vortices into the sample, leads to history dependent effects. The curves in Fig. 2 were generated increasing the field H_{dc} at low frequency and then measuring $\chi''(\omega)$ for increasing ω. In this way, the curves reported in Fig. 2(c) have the same number of vortices at all frequencies for a given H_{dc}. If we follow the opposite procedure, i.e., we increase H_{dc} at high frequency and then measure $\chi''(\omega)$ for decreasing ω, the curves can show discontinuous jumps at certain frequencies values due to vortex penetration. This occurs because increasing the field at high frequency can generate a metastable state that can become unstable at low frequencies. In Fig. 5 we show this case, for a field near the first penetration field $H_{dc}\approx H_p$. Depending on the history, the high-frequency branch can have either $N_v=10$ vortices or $N_v=0$. In the case when the frequency is decreased from a high-frequency state, there is a large jump in $\chi''(\omega)$ at a frequency near ω_p, from a metastable branch with $N_v=0$ for $\omega>\omega_p$ to a branch with $N_v=10$ for $\omega<\omega_p$. In contrast, we see in the inset of Fig. 5 that for a field $H_{dc}\neq H_p$ the curves of $\chi''(\omega)$ are independent of history.

B. Magnetic-field dependence

Experimentally, the ac frequency is fixed and the dc magnetic field or the temperature can be varied. In this section we will study the ac magnetic response of mesoscopic superconductors varying the bias dc magnetic field. We will show results at different frequencies and for different sample sizes.

In the absence of the ac field, the dc magnetic behavior of mesoscopic superconductors is different from the continuous macroscopic behavior.[16,29] In mesoscopic samples each vortex entrance event produces discontinuous jumps in the magnetization curve at certain H_{dc} values. Each discontinuous jump in $M(H)$ corresponds to a sudden increase in the number of vortices. These jumps occur at successive magnetic fields $H_{pi}=H_{p1},H_{p2},H_{p3},\ldots$.[29] In the regions of $H_{pi}<H<H_{p(i+1)}$ the number of vortices N_v is constant. The only penetration events occur at H_{pi}, when vortices enters into the sample. In the region of constant vorticity, $H_{pi}<H<H_{p(i+1)}$, one may think that no vortices enter the sample because of the effect of the surface barrier.

Figure 6(a) shows the behavior of $\chi''(H_{dc})$ obtained at a fixed frequency $\omega=0.004\nu_o<\omega_p$ in a mesoscopic sample of size $10\lambda\times10\lambda$. At small H_{dc}, in the Meissner state, χ'' increases continuously with increasing H_{dc}. The presence of the dc magnetic field in the Meissner state induces static supercurrents which deplete the order parameter at the boundary. As explained before in Sec. IV A, the depletion of the order parameter leads to an increase of dissipation for increasing H_{dc}. When the dc magnetic field is increased above the first penetration field $H_p\equiv H_{p1}$, the first vortices enter into the sample. Figure 6(a) shows that there is a discontinuous jump in χ'' with a decrease of dissipation just at H_p. Two states are possible exactly at H_p: one state without vortices and high dissipation, and one state with vortices inside the sample and *low* dissipation. This is in agreement with the history dependence observed in Fig. 5. Further jumps in the dissipation curve $\chi''(H_{dc})$ are present at the other magnetic fields for vortex penetration, $H_{p2},H_{p3},\ldots$. The jumps are followed by a later continuous increase of $\chi''(H_{dc})$ with increasing H_{dc} while the number of vortices N_v remains fixed. Figure 6(b) was obtained in a sample of the same size of Fig. 6(a) but at a higher frequency $\omega=0.06\nu_o>\omega_p$. The frequencies used in Figs. 6(a) and (b) are at both sides of the dissipation maximum that appears at ω_p. Both curves are similar in their qualitative features, but show a few differences. At high magnetic fields there are fewer jumps in $\chi''(H_{dc})$ in Fig. 6(b) than in Fig. 6(a). This is because at high frequencies it is possible to remain in a metastable state with a fixed number of vortices in a wider range of magnetic field. At the same time, the higher frequency of Fig. 6(b) produces a decrease in the amplitude of the jumps. The behavior of $\chi''(H_{dc})$ of Figs. 6(a) and (b) is different from the behavior of bulk samples. For example, Fig. 6(c)

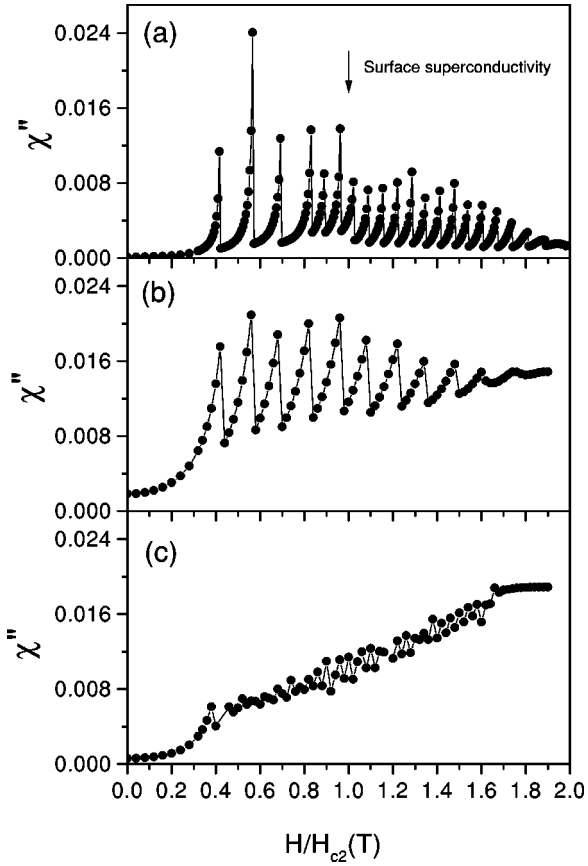

FIG. 6. H_{dc} dependence of χ'' obtained at a fixed frequency. Small mesoscopic samples of size $10\lambda \times 10\lambda$ showing discontinuous jumps: (a) $\omega t_0 = 0.004$ and (b) $\omega t_0 = 0.06$. (c) Large samples of size $40\lambda \times 40\lambda$ showing the usual continuous behavior, $\omega t_0 = 0.06$.

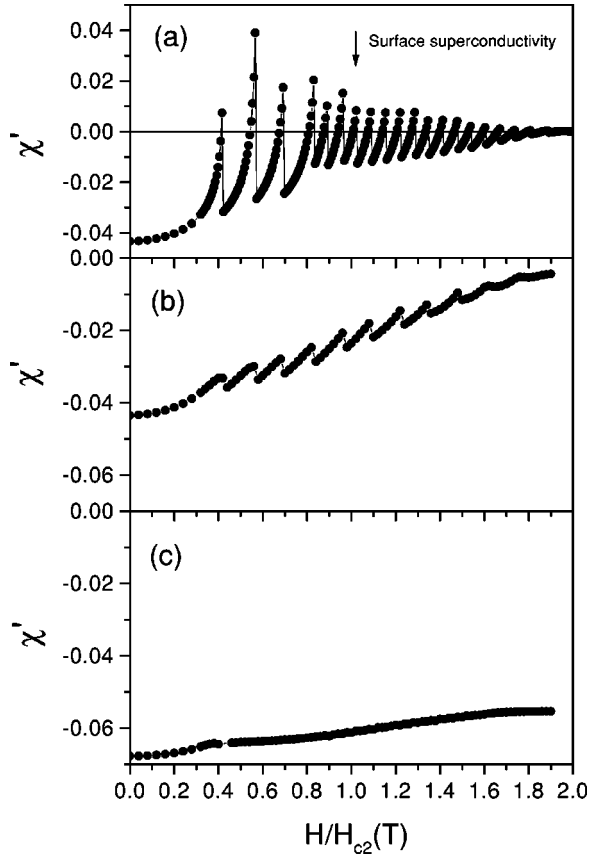

FIG. 7. H_{dc} dependence of χ' obtained at a fixed frequency: (a) and (b) for small samples and (c) for large samples. The parameters are the same as used in Fig. 6.

shows $\chi''(H_{dc})$ at $\omega = 0.06\nu_o$ obtained in a ''large'' sample of $40\lambda \times 40\lambda$. In this case there are no discontinuous jumps and the curve is almost continuous. In macroscopic samples the entrance of vortices for $H_{dc} > H_p$ increases the ac losses in a continuous way. In the macroscopic case vortices play a fundamental role in the ac losses, and therefore an increase on the number of vortices increases the dissipation. In contrast, the results of Figs. 6(a) and (b) show the opposite behavior in mesoscopic samples: there is a sudden decrease of the ac losses at the magnetic fields that correspond to an increase in the number of vortices.

Figure 7 shows the real part of the ac susceptibility for increasing H_{dc}. We use the same parameters as in Fig. 6. The curves of $\chi'(H_{dc})$ also have a typical mesoscopic behavior with discontinuities at each vortex penetration field. The increase of frequency from $\omega = 0.004\nu_o$ in Fig. 7(a) to $\omega = 0.06\nu_o$ in Fig. 7(b) shows similar differences as observed in $\chi''(H_{dc})$. It can also be noted in Fig. 7(a) that the differential susceptibility has a paramagnetic behavior ($\chi' > 0$) near each vortex penetration field. This can be expected from the behavior of the dc magnetization curves of mesoscopic samples.[16] In mesoscopic samples, for H_{dc} below each vortex penetration field a magnetization maximum appears and therefore a region near H_{pi} where the magnetization increases at increasing field. This shows in the low-frequency ac response of mesoscopic samples as a differential paramagnetic behavior. Figure 7(c) shows a continuous macroscopic dependence of $\chi'(H_{dc})$ in a larger sample of size $40\lambda \times 40\lambda$. At the frequencies used in Fig. 7(c) we can see a diamagnetic behavior even in the normal state for fields greater than $2H_{c2}(T)$. This is simply because at high frequencies there is magnetic screening in the normal state due to the skin depth effect.

From Fig. 7 it is possible to obtain the H_{dc} dependence of the penetration depth. This dependence has been a subject of interest recently because of its relation with the symmetry of the order parameter. In conventional *s*-wave superconductors the following dependence is expected:

$$\Delta\lambda(H_{dc},T)/\lambda(0,T) = \beta[H_{dc}/H_{c2}(T)]^2, \qquad (21)$$

where $\Delta\lambda(H_{dc},T) = \lambda(H_{dc},T) - \lambda(0,T)$. It is assumed that the sample is in the Meissner state and in the linear regime, i.e., $|H_{dc}| \gg |h_{ac}|$. Equation (21) was originally obtained by Ginzburg and Landau[51] and also by Bardeen[52] an it has been observed experimentally in type-I (Refs. 1 and 3) and conventional type-II superconductors.[10] Solving the Ginzburg-Landau equations for a superconductor which has an infinite plane interface, the value $\beta_{GL} = [3\kappa^3(\kappa + 2\sqrt{2})]/[4(\kappa + \sqrt{2})^2]$ is obtained. On the other hand, the behavior of $\Delta\lambda(H)$ in unconventional superconductors is expected to be

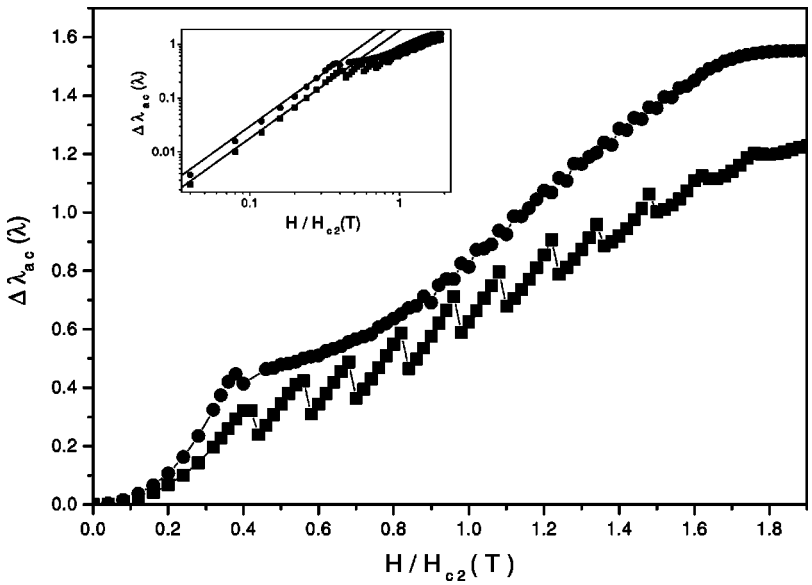

FIG. 8. Change in the ac penetration depth ($\Delta\lambda_{ac}$) in a mesoscopic sample (squares, $10\lambda \times 10\lambda$) and a macroscopic sample (circles, $40\lambda \times 40\lambda$) for $\omega t_0 = 0.06$. The inset shows a fit to a quadratic dependence $\Delta\lambda_{ac} \sim H^2$ (continuous lines) for fields below H_p.

different.[14] In the case of a *d*-wave superconductor Yip and Sauls[53,54] proposed a linear field dependence $\Delta\lambda(H_{dc}) \propto H_{dc}$. Here we use the phenomenological TDGL equation in its *s*-wave form. Therefore in the Meissner state we expect a result similar to Eq. (21) for macroscopic samples. The results are shown in Fig. 8. Both the macroscopic and the mesoscopic sample show a quadratic dependence of $\Delta\lambda(H_{dc})$ as a function of H_{dc} in the Meissner state. We obtain from the macroscopic curve $\beta \approx 3.1$, which is close to the expected Ginzburg-Landau value $\beta_{GL} = 2.48$ for $\kappa = 2$. For larger magnetic fields we observe that the penetration of vortices produces a sudden decrease of $\Delta\lambda$ in mesoscopic samples, whereas at a fixed number of vortices $\Delta\lambda$ increases continuously for increasing H_{dc}. For macroscopic samples the entrance of vortices at the first penetration field H_p does not produce a discontinuity in $\Delta\lambda(H_{dc})$ but a change of slope as can be observed in the plot. For $H_{dc} > H_p$ the dependence changes from quadratic to approximately linear in H_{dc}.

V. NASCENT VORTICES EFFECT

From the results of the previous section, it is clear now that the ac magnetic response of a mesoscopic superconductor is different from the macroscopic behavior and it cannot be explained with the known models. An interesting result is the significant decrease of dissipation each time the number of vortices increases. To understand this effect we have analyzed in detail the time variation of the order parameter and the magnetization within the sample.

Figure 9 shows the time variation of the order parameter at different applied magnetic fields in a small sample. Each curve represents the amplitude of the order parameter along the *x* direction, perpendicular to a face of the square sample, obtained at a given time. To simplify the analysis the cut was done just at the center of the face at $y = L/2$ (which is the preferred point for vortex penetration in a square sample). The order parameter is obtained at different times within a single period of the ac magnetic field. In particular, we show the behavior of the order parameter just before and after the two first values of the penetration fields, H_{p1} and H_{p2}. At $H_{dc} = 0$ the order parameter $|\Psi|$ is equal to unity in the entire sample and the dissipation is small. In the Meissner state but for $H_{dc} \lesssim H_{p1}$, Fig. 9(a) shows that the magnitude of the order parameter near the boundary, and at the center of the face, has large oscillations around a small value. Figure 9(b) shows the time evolution of order parameter just after the first vortex entrance event, $H_{dc} \gtrsim H_{p1}$. We see that the entrance of vortices increases the order parameter at the boundary, where now $|\Psi|$ oscillates around a value much higher than before. One can also see that the positions of the vortices are fixed inside the sample and do not oscillate in the presence of the ac signal. Recently, in an extension of the idea of the Bean-Livingston barrier to mesoscopic superconductors, we have shown that the vortex entrance produces a reinforcement of the surface barrier, due to the interaction between the vortices that are trying to enter the sample and the vortices already inside the sample.[29] The presence of this interaction decreases the surface currents. In other words, after the entrance of vortices the Meissner screening current decreases and the amplitude of the order parameter increases at the boundary. Therefore, the dissipation decreases.

Figures 9(c) and (d) show similar behavior for $H_{dc} \lesssim H_{p2}$ and $H_{dc} \gtrsim H_{p2}$. After increasing H_{dc} at a constant number of vortices, the order parameter at the boundary has decreased, as seen in Fig. 9(c). The decrease of the order parameter increases the dissipation as was observed before. If new vortices enter again into the sample, the order parameter increases at the boundary, see Fig. 9(d) and therefore the dissipation decreases again. This process is repeated in the other penetration fields H_{pi}. On the contrary, the entrance of vortices in a large sample do not produce an appreciable change in the amplitude of the order parameter at the boundary before and after the penetration event, and therefore the dissipation shows a continuous behavior [as seen in Fig. 6(c)].

A careful analysis of the entire profile of the order parameter for magnetic fields below but near to H_p suggest that the

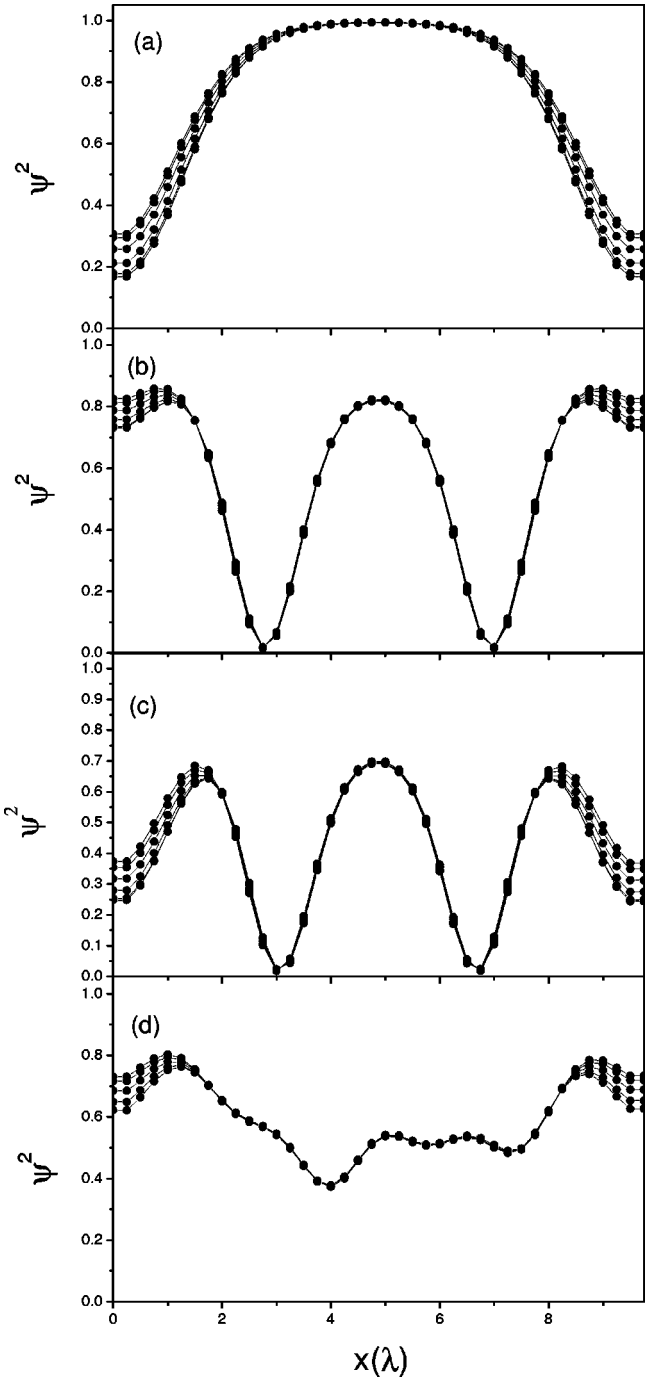

FIG. 9. Time variation of the order parameter in a sample of size $10\lambda \times 10\lambda$ at different applied magnetic fields and for $\omega t_0 = 0.06$. The figures show transversal cuts taken at the center of one of the faces for different times. (a) $H_{dc} = 0.4216 H_{c2}(T) < H_{p1}$, (b) $H_{dc} = 0.4217 H_{c2}(T) > H_{p1}$, (c) $H_{dc} = 0.568 H_{c2}(T) < H_{p2}$, (d) $H_{dc} = 0.569 H_{c2}(T) > H_{p2}$.

depletion of the order parameter near the boundary may be attributed to ''vortices'' that are about to enter into the sample. This is because the profile of the depletion of $|\Psi|$ observed at the boundary can be easily extrapolated to a zero value outside of the sample. Therefore these ''nascent vortices'' correspond, in a sense, to the order parameter profile $|\Psi(r)|$ that one would obtain if hypothetical vortices were located in the vacuum, beyond the sample boundary, but near the surface. Note that since $|\Psi|$ does not truly have a zero inside the sample, the topological number of vorticity, $N_v = (1/\Phi_o) \oint (A + J_s/|\Psi|^2) dl$, is $N_v = 0$ and thus there is no fluxoid quantization. Indeed, a nascent vortex state corresponds to the penetration of less than a flux quantum. For high values of h_{ac} (beyond linear response) we find that these nascent vortices oscillate near the surface [i.e., that the profile of the depletion of $|\Psi|$ near the surface oscillates with $H(t)$]. Also, from the simulations we obtain that for increasing H_{dc} the nascent vortices gradually transform into the real vortices that finally enter the sample (and that satisfy fluxoid quantization). According to this scenario, the length scale l_p observed in Fig. 3(b) for low frequencies may correspond to a characteristic length scale for the nucleation of vortices from the boundary. (For large fields $B \gg H_p$, the length l_p could be related to the size of the vortex-free region d_{SB} of macroscopic samples.) Years ago, Walton and Rosemblum[55] introduced the idea of nascent vortices and suggested them as a possible source of the high-frequency losses in superconductors. This idea had further support from the analytical work of Kramer[56] who found static solutions of the Ginzburg-Landau equations which corresponded to vortices nucleated near the sample. The nascent vortices can oscillate under an ac field. This source of dissipation is not generally taken into account in macroscopic samples because in this case it is small compared with the dissipation due to the motion of vortices inside the sample. However, in a mesoscopic superconductor, with a few vortices confined inside the sample, this source of dissipation can be a significant part of the dissipation observed, as we have found here.

VI. SUMMARY AND CONCLUSION

We have studied the response of mesoscopic superconductors to an ac magnetic field. In mesoscopic superconductors vortices are confined inside the sample by the surface barrier and their dynamics play a secondary role in the dissipation. When increasing H_{dc}, discontinuities in χ' and χ'' appear at each vortex penetration event. The dissipation is maximum before the penetration of vortices due to the effect of nascent vortices, which lead to large oscillations of the amplitude of the order parameter at the boundary. After the penetration of vortices, the normal currents decrease and therefore the dissipation decreases, leading to a sudden suppression of the ac losses induced by the vortex entrance.

ACKNOWLEDGMENTS

A.D.H. acknowledges Oscar Arés and C. Hart for useful comments and help and the Centro Latino-Americano de Física (CLAF) for financial support. D.D. acknowledges support from Conicet and CNEA. We acknowledge financial support from the Argentina-Cuba cooperation Project No. SETCIP-CITMA: CU/A00-EIII/005 and from ANPCyT (Argentina) Project No. PICT99-03-06343.

[1] A. B. Pippard, Proc. R. Soc. London, Ser. A **203**, 210 (1950).
[2] J. R. Clem, H. R. Kerchner, and S. T. Sekula, Phys. Rev. B **14**, 1893 (1976).
[3] S. Sridhar and J. E. Mercereau, Phys. Rev. B **34**, 203 (1986).
[4] M. W. Coffey and J. R. Clem, Phys. Rev. Lett. **67**, 386 (1991); Phys. Rev. B **45**, 9872 (1992).
[5] E. H. Brandt, Phys. Rev. Lett. **67**, 2219 (1991); Physica C **185-189**, 270 (1991).
[6] V. B. Geshkenbein, V. M. Vinokur, and R. Fehrenbacher, Phys. Rev. B **43**, 3748 (1991).
[7] C. J. van der Beek, V. B. Geshkenbein, and V. M. Vinokur, Phys. Rev. B **48**, 3393 (1993).
[8] E. B. Sonin and K. B. Traito, Phys. Rev. B **50**, 13 547 (1994).
[9] S. Sridhar, D. Wu, and W. Kennedy, Phys. Rev. Lett. **63**, 2264 (1989).
[10] T. Hanaguri, Y. Iino, A. Maeda, and T. Fukase, Physica C **246**, 223 (1995); A. Maeda, Y. Iino, T. Hanaguri, N. Motohira, K. Kishio, and T. Fukase, Phys. Rev. Lett. **74**, 1202 (1995).
[11] R. Mallozzi, J. Orenstein, J. N. Eckstein, and I. Bozovich, Phys. Rev. Lett. **81**, 1485 (1998).
[12] Alan M. Portis, *Electrodynamics of High-Temperature Superconductors* (World Scientific, Singapore, 1993).
[13] F. Gömöry, Supercond. Sci. Technol. **10**, 523 (1997).
[14] A. Maeda, in *Coherence in High Temperature Superconductors*, edited by G. Deutscher and A. Revcolevschi (World Scientific, Singapore, 1995), p. 128; A. Maeda and T. Hanaguri, Supercond. Rev. **3**, 1 (1998).
[15] O. Buisson, P. Gandit, R. Rammal, Y. Y. Wang, and B. Pannetier, Phys. Lett. A **150**, 36 (1990).
[16] C. Bolech, G. C. Buscaglia, and A. López, Phys. Rev. B **52**, R15 719 (1995).
[17] C. A. Bolle, V. Aksyuk, F. Pardo, P. L. Gammel, E. Zeldov, E. Bucher, R. Boie, D. J. Bishop, and D. R. Nelson, Nature (London) **399**, 43 (1999).
[18] A. K. Geim *et al.*, Nature (London) **396**, 144 (1998).
[19] A. K. Geim, S. V. Dubonos, I. V. Grigorieva, F. M. Peeters, and V. A. Shweigert, Nature (London) **407**, 55 (2000).
[20] P. Singha Deo, V. A. Shweigert, F. M. Peeters, and A. K. Geim, Phys. Rev. Lett. **79**, 4653 (1997).
[21] V. A. Shweigert, F. M. Peeters, and P. Singha Deo, Phys. Rev. Lett. **81**, 2783 (1998).
[22] V. A. Shweigert and F. M. Peeters, Phys. Rev. B **60**, 3084 (1999).
[23] B. J. Baelus, F. M. Peeters, and V. A. Shweigert, Phys. Rev. B **61**, 9734 (2000).
[24] P. Singha Deo, V. A. Shweigert, and F. M. Peeters, Phys. Rev. B **59**, 6039 (1999).
[25] S. V. Yampolskii, B. J. Baelus, V. A. Shweigert, and J. Kolacek, Phys. Rev. B **64**, 144511 (2001).
[26] J. J. Palacios, Phys. Rev. Lett. **84**, 1796 (2000).
[27] V. Bruyndoncx, J. G. Rodrigo, T. Puig, L. Van Look, and V. V. Moshchalkov, Phys. Rev. B **60**, 4285 (1999).
[28] L. F. Chibotaru, A. Ceulemans, V. Bruyndoncx, and V. V. Moshchalkov, Nature (London) **408**, 833 (2000).
[29] A. D. Hernández and D. Domínguez, Phys. Rev. B **65**, 144529 (2002).
[30] C. P. Bean and J. D. Livingston, Phys. Rev. Lett. **12**, 14 (1964).
[31] H. Frah, S. Ulah, and A. T. Dorsey, Phys. Rev. Lett. **66**, 3067 (1991).
[32] F. Liu, M. Mondelo, and N. Goldenfeld, Phys. Rev. Lett. **66**, 3071 (1991).
[33] R. Kato, Y. Enomoto, and S. Maekawa, Phys. Rev. B **47**, 8016 (1993).
[34] M. Machida and H. Kaburaki, Phys. Rev. Lett. **71**, 3206 (1993); M. Machida and H. Kaburaki, Phys. Rev. B **50**, 1286 (1994).
[35] I. Aranson, M. Gitterman, and B. Ya. Shapiro, Phys. Rev. B **51**, 3092 (1995).
[36] I. Aranson, B. Ya. Shapiro, and V. Vinokur, Phys. Rev. Lett. **76**, 142 (1996).
[37] I. Aranson and V. Vinokur, Phys. Rev. Lett. **77**, 3208 (1996).
[38] Y. Enomoto and K. Okada, J. Phys.: Condens. Matter **8**, L445 (1996); Y. Enomoto, Y. Ishikawa, and S. Maekawa, Physica C **263**, 21 (1996); Y. Enomoto and K. Okada, J. Phys.: Condens. Matter **9**, 10 203 (1997).
[39] J. J. Vicente Álvarez, D. Domínguez, and C. A. Balseiro, Phys. Rev. Lett. **79**, 1373 (1997).
[40] W. D. Groop, H. G. Kaper, G. L. Leaf, D. M. Levine, M. Palumbo, and V. M. Vinokur, J. Comput. Phys. **123**, 254 (1996).
[41] D. Schoenberg, *Superconductivity* (Cambridge University Press, Cambridge, England, 1952), p. 197.
[42] J. I. Gittleman and B. Rosenblum, Phys. Rev. Lett. **16**, 734 (1966).
[43] For an estimate of time scales in the TDGL equations see, for example, A. M. Kadin and A. M. Goldman, in *Nonequilibrium Superconductivity*, edited by D. N. Langenberg and A. I. Larkin (North-Holland, Amsterdam, 1986), p. 253.
[44] J. R. Clem, in *Proceedings of the 13th Conference on Low Temperature Physics* (LT13), edited by K. D. Timmerhaus, W. J. O'Sullivan, and E. F. Hammel (Plenum, New York, 1974), Vol. 3, p. 102.
[45] F. F. Ternovskii and L. N. Shekhata, Zh. Éksp. Teor. Fiz. **62**, 2297 (1972) [Sov. Phys. JETP **35**, 1202 (1972)].
[46] L. Burlachkov, Phys. Rev. B **47**, 8056 (1993).
[47] L. Fabrega, A. Sin, A. Calleja, and J. Fontcuberta, Phys. Rev. B **61**, 9793 (2000).
[48] N. Morozov, E. Zeldov, D. Majer, and B. Khaykovich, Phys. Rev. Lett. **76**, 138 (1996).
[49] A. Schmid, Phys. Kondens. Mater. **5**, 302 (1966); C. R. Hu and R. S. Thompson, Phys. Rev. B **6**, 110 (1972); A. T. Dorsey, *ibid.* **46**, 8376 (1992).
[50] L. P. Gorkov and G. M. Eliashberg, Zh. Eksp. Teor. Fiz. **54**, 612 (1968) [Sov. Phys. JETP **27**, 328 (1968)].
[51] V. L. Ginzburg and L. D. Landau, J. Exp. Theor. Phys. **20**, 1064 (1950).
[52] J. Bardeen, Phys. Rev. **94**, 554 (1954).
[53] S. K. Yip and J. A. Sauls, Phys. Rev. Lett. **69**, 2264 (1992).
[54] D. Xu, S. K. Yip, and J. A. Sauls, Phys. Rev. B **51**, 16 233 (1995).
[55] B. L. Walton and B. Rosemblum, *Proceedings of the 13th International Conference on Low Temperature Physics* (Plenum Press, New York, 1972), p. 172; B. L. Walton, B. Rosemblum, and F. Bridges, Phys. Lett. **43A**, 263 (1973).
[56] L. Kramer, Z. Phys. **259**, 333 (1973).